Research Article | Vol. 29, No. 26 / 20 Dec 2021 / Optics Express 42538
Optics EXPRESS

On the measurement accuracy of coherent Rayleigh-based distributed sensors

MALAK GALAL,[1,2,3] SUNEETHA SEBASTIAN,[1,2,4] ZHISHENG YANG,[1] LI ZHANG,[1] SIMON ZASLAWSKI,[1] AND LUC THÉVENAZ[1]

[1]Ecole Polytechnique Fédérale de Lausanne, SCI-STI-LT Station 11, 1015 Lausanne, Switzerland
[2]Both authors contributed equally to this work
[3]malak.galal@epfl.ch
[4]suneetha.sebastian@epfl.ch

Abstract: The phase change of back-scattered light due to external perturbations is retrieved in coherent Rayleigh-based distributed sensors by estimating the frequency shift (FS) between the traces of different measurements. The uncertainty associated with the estimator, due to the presence of system noises, can lead to an inaccurate evaluation of the FS. Additionally, in coherent Rayleigh-based sensors, the calculation of the signal-to-noise ratio (SNR) from the jagged back-scattered intensity trace using the statistical estimators can cause an erroneous determination of the absolute value of the SNR. In this work, a method to accurately evaluate the non-uniform SNR caused by the stochastic variation of the back-scattered light intensity along the fibre is presented and validated. Furthermore, an analytical expression to evaluate the uncertainty in the FS estimation using one of the standard estimators, namely cross-correlation, is presented. A direct-detection frequency-scanned phase-sensitive optical time-domain reflectometer (φ-OTDR) is employed for the experimental verification of the expression as a function of two crucial system parameters: the SNR and the spatial resolution. The performance of various distributed sensing system configurations utilising cross-correlation for determining the FS occurring due to the external perturbations can be properly predicted hereafter with the aid of the analytical expression presented in this study.

1. Introduction

Over the past 50 years, distributed optical fibre sensors (DOFS) have received unprecedented attention owing to their benefits in terms of long-haul detection, intrinsic safety, flexibility, immunity to electromagnetic interference, and low cost [1,2]. Among the various types of DOFS, distributed optical sensing based on Rayleigh scattering demonstrates a significantly high sensitivity to external perturbations with frequency shifts of 1.3 GHz/K and 150 kHz/nϵ for temperature and strain variations [3], respectively, outperforming systems based on Brillouin scattering by at least 3 orders of magnitude. However, the enhanced sensitivity of such systems to the external fluctuations, along with the inevitable system noises, can affect the system performance through less reliable measurements. In addition, the Rayleigh back-scattered light, a universal signal present in all types of optical fibres, is a feeble signal (with a back-scattering coefficient of ~ −72 dB/m for a standard single-mode fibre) which can potentially limit the system performance through low SNR thereby impeding high spatial resolution measurements.

Several approaches have been discussed in the literature with the goal of optimising the performance of DOFS based on coherent Rayleigh scattering through the ultimate parameter, the SNR. Improving the SNR of a system can dramatically scale up its performance in terms of sensing range, accuracy of the measurement, speed of acquisition, spatial resolution, along with others [4]. A few methods employed for this purpose are conventional temporal averaging,

#442790 https://doi.org/10.1364/OE.442790
Journal © 2021 Received 7 Sep 2021; revised 25 Nov 2021; accepted 25 Nov 2021; published 7 Dec 2021

Optics EXPRESS

spatial averaging [5], increasing the power of the launched pulse directly or with pulse coding achieving an SNR enhancement of 8 dB [6,7], enhancing the back-scattered signal through Raman amplification [8,9], data processing methods [10,11] increasing the SNR by 8.4 dB and 8.5 dB, respectively, and enhancing the back-scattered light by manipulating the scattering properties of the fibre [12–14] achieving an SNR as high as ~ 35 dB [2]. Alongside the prodigious effort made to achieve SNR enhancement, several works extensively discussed the possibility to resolve the physical alterations at the sub-metre scale which will substantially improve the accuracy in the determination of the exact location of the external perturbation [15,16].

Despite the tremendous work that has been carried out aiming at ameliorating the system performance of Rayleigh-based DOFS through interdependent parameters such as SNR and spatial resolution, a proper relationship pertaining the dependency of these parameters on the measurement accuracy has not been properly addressed yet. For Brillouin-based DOFS, a comprehensive model has been derived to estimate the FS uncertainty of the Brillouin gain spectrum with respect to various measurement parameters [17]. The derived model is valid for any system for which the peak value of a resonance is evaluated through quadratic least-square fitting. In the case of coherent Rayleigh-based DOFS, for instance in direct-detection frequency-scanned φ-OTDR systems, the most widely and commonly-used method to estimate the relative value of the FS between reference and measurement signals is cross-correlation [18–20]. Cross-correlation is a standard method utilised for delay estimation in sonar and radar systems [21–23], and is also adopted in other coherent Rayleigh-based DOFS [24]. The presence of unavoidable additive noise in the traces being correlated fundamentally limits the performance of the cross-correlation estimator and leads to uncertainty in the estimated FS. Besides, other experimental parameters, such as spatial resolution, can also influence the accuracy of estimation.

Due to the presence of stochastic refractive index fluctuations along the fibre, the Rayleigh back-scattered intensity received from each location in the fibre in φ-OTDR, results from the coherent superposition of numerous elementary waves with random phase, constructs a jagged noise-like pattern. Due to the non-uniform distribution of the received scattered intensity along the fibre, the calculation of the SNR of the system from the intensity distribution is highly subjected to errors. This study presents a method to calculate the absolute value of the SNR from the jagged φ-OTDR intensity trace, which turns out to be critical to make solid predictions and to require a peculiar methodology.

This paper, thus, addresses in depth the fundamental question of predicting the accuracy of the Rayleigh-based distributed sensing system on the measured quantity, given experimental parameters such as the local SNR and the spatial resolution. Even though most of the fibre sensing systems show a simple dependence in inverse proportion to the SNR, such as those based on Raman and Brillouin scatterings, it must be mentioned that stating an equivalent dependence for coherent Rayleigh systems is not that straightforward, since the information is extracted from a mathematical operation of cross-correlation involving two independent traces, both subject to noise. To demonstrate this, an analytical expression based on the concept of time-delay estimation using cross-correlation in radar and sonar systems [21–23] is well adapted to the present scenario and evaluated for determining the accuracy of the FS estimation employing cross-correlation in φ-OTDR. It will be shown and experimentally validated that this inverse proportionality remains also valid in coherent Rayleigh distributed sensors, while the spatial resolution impacts twice on the accuracy through the SNR and the correlation peak spectral width, resulting in an inverse squared dependence of the uncertainty on the spatial resolution. The analytical expression can be applied to any system wherein the measurand is quantified through cross-correlation.

Optics EXPRESS

2. Expression for estimating the measurement accuracy

2.1. Direct-detection frequency-scanned φ-OTDR

Direct-detection frequency-scanned φ-OTDR retrieves the phase information of the back-scattered light at each position in the fibre through laser frequency (f) scanning with a specified step size (Δf) [25] (Fig. 1(a)) followed by data processing. The methodology consists of interrogating the fibre with highly coherent laser pulses, with a pulse width determined by the desired spatial resolution of the measurement. The period of the pulses is made greater than the round trip time of the pulse in the fibre, and the pulse optical carrier frequency is scanned over a preset frequency range. The statistical distribution of coherent Rayleigh back-scattered intensity follows an identical process as the generation of chaotic light, formally equivalent to a random walk process, so that the normalised back-scattered intensity pattern received at the photo-detector follows an exponentially decaying distribution [26]. The back-scattered optical intensity measured by the photo-detector for each fibre location is thus a function of time (or equivalently a function of distance, as shown in Fig. 1(b)), and the pulse laser optical frequency. Accordingly, a 2-D array is constructed having the columns as the different positions throughout the sensing fibre, and the rows as the scanned frequencies, which is illustrated on the upper part of Fig. 1(c). The intensity of the light received at the photo-detector corresponding to each pulse at a specified frequency of the laser constructs an irregular time-domain trace along the whole length of the fibre (Fig. 1(b)). Such a trace corresponding to a particular frequency and a row in the array in Fig. 1(c) can be considered as a fingerprint of the fibre as it is static under constant environmental conditions.

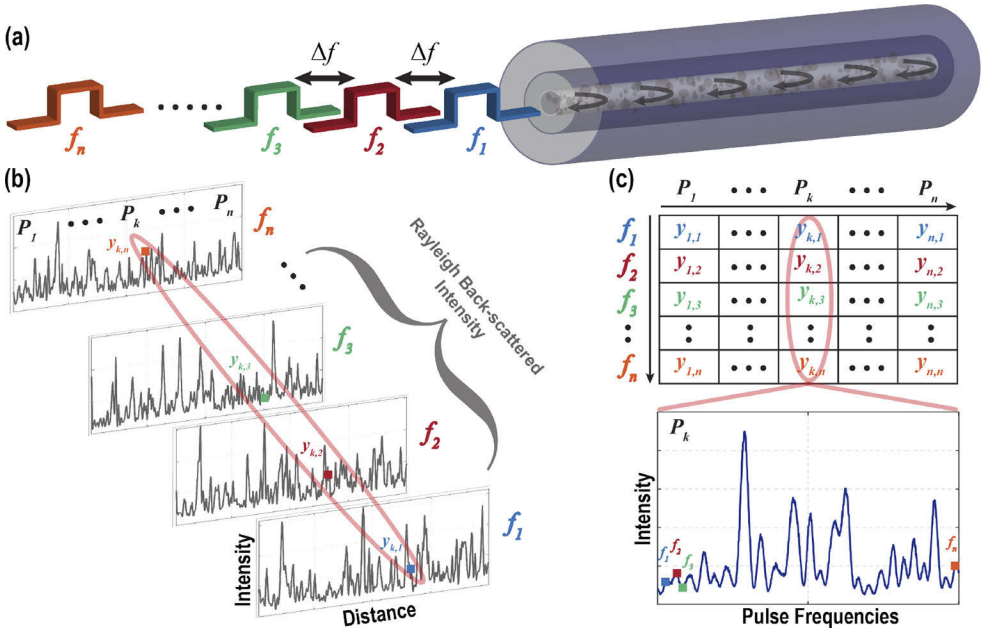

Fig. 1. Concept of frequency-scanned φ-OTDR: (a) Schematic showing optical pulses at different frequencies separated by a frequency scan step of Δf shot in a standard single-mode fibre one at a time, (b) Rayleigh back-scattered intensity time-domain traces corresponding to the different pulse frequencies entering the fibre, (c) Upper figure: Experimentally obtained 2-D array containing the different positions along the sensing fibre (columns) for different frequencies in the scanning range (rows); (P_1-P_n: positions, f_1-f_n: frequencies); Bottom figure: Back-scattered intensity corresponding to a specific position in the fibre for all the different pulse frequencies.

Optics EXPRESS

The information in the array can be also interpreted column-wise and it similarly appears like a jagged trace, representing the coherent Rayleigh spectral response at a given position (shown in the lower portion of Fig. 1(c)) and will be designated hereafter as the *artificially-constructed signal*. Indeed this signal is a spectral response and is not measured directly, but artificially extracted from a set of time-domain traces.

Optical phase difference created by the localised external perturbations changes the pattern of the artificially-constructed trace at this specified location as the optical path length of the propagating light is changed as a consequence of the variation of refractive index that causes a phase change on each elementary wave resulting in an effect equivalent to a frequency change. This phase difference can thus be fully restored through an appropriate optical FS of f, which then provides a direct indication of the local refractive index change at that location. One of the most commonly-used methods in φ-OTDR to determine the FS caused by the localised external perturbation acting along the fibre, is to compute the cross-correlation function between the artificially-constructed reference trace (x_r) and a subsequent measurement trace (x_m) which is given by [15]:

$$\hat{R}_{x_r,x_m}(\delta f) = \frac{1}{F}\sum_{i=1}^{F} x_r(f_i)\, x_m(f_i - \delta f) \tag{1}$$

These signals are formed by the optical intensity values of the φ-OTDR time-domain signals at one particular fibre position for all the pulse frequencies in the scanning range (depicted in the lower portion of Fig. 1(c)). F is the number of frequencies in the total frequency-scan range of the laser, δf is the FS that has to be determined. The value of δf that maximises the above function, designated as δf^{max}, provides a measured value of the FS. The accuracy with which the FS can be estimated is influenced by a number of parameters. Hence, the uncertainty in the estimation (FS uncertainty, σ) can be considered as the difference between the measured value (δf^{max}) and the true value estimated independently of the same set of measurements ($\hat{\delta f}^{max}$) of the FS which can be formulated as:

$$\sigma = \sqrt{\frac{1}{I}\sum_{m=1}^{I}(\delta f^{max}_{x_{r,m+1}} - \hat{\delta f}^{max}_{x_{r,m+1}})^2} \tag{2}$$

where I is the total number of measurements. In the case when the true value is not independently known, but is estimated from the same experimental sample of data, the normalising factor will be $\frac{1}{I-1}$ instead. The index of that value ($x_{r,m+1}$) will no longer be relevant in that case.

It should be noted that the signals used for cross-correlation are artificially constructed, and that there is no mathematical difference whatsoever between considering these signals to be physically in any particular domain. They can be simply regarded as signals with a specific number of samples in no defined domain, indicating that the physical quantity represented on the x-axis is completely irrelevant for the estimation. Consequently, the FS estimation can be approached in a similar manner as a time-delay estimation problem just like in the case of sonar and radar systems [21–23].

2.2. Measurement accuracy estimation for a rectangular input pulse

Due to the presence of inevitable measurement noises, the cross-correlation estimator comprises uncertainty which needs to be taken into consideration during the estimation. All sources of noise in the system can be considered as zero-mean additive white Gaussian noise to the original signal. In turn, the paper solely addresses uncertainty due to system noises. Any additional ambiguities in the estimation, like laser frequency drifting or large errors resulting from correlation for instance, do not result from noise and, hence, have to be addressed independently as elaborated in great detail in one of the previous studies [15]. The estimated uncertainty in the FS determination

Optics EXPRESS

is given by Eq. (2). Since the Rayleigh back-scattering can be considered as a random process [27–29], a probabilistic model can be followed to obtain an expression for the uncertainty in the determination of the FS using cross-correlation as presented in [30–34] in the case of time-domain radar signals. Eventually, considering the mathematical equivalence between the time-delay estimation in the case of the sonar and the radar systems and the FS estimation in the present scenario, the expression for the uncertainty with which the FS can be determined is given as [33,35]:

$$\sigma = \frac{1}{\beta\sqrt{M_e}} = \frac{1}{\beta M_o} \tag{3}$$

where M_o represents the SNR calculated using the optical power and the parameter β represents the square root of the second moment β^2 of the power density $|U(f)|^2$ of the artificially-constructed signal $u(x)$ expressed as follows:

$$\beta^2 = 4\pi^2 \frac{\int f^2 |U(f)|^2 df}{\int |U(f)|^2 df} \tag{4}$$

where f is the laser frequency and $U(f)$ is the Fourier transform of $u(x)$.

It should be noted that the SNR for the optical power of the signal is equivalent to the square root of the SNR of the electrical power M_e. In the present case of direct-detection frequency-scanned φ-OTDR, the SNR (M_o) is calculated using the power of the optical signal received at the photo-detector. Consequently, the dependence of σ on the SNR is inverse as shown in Eq. (3). The handling of the artificially-constructed signal, and the proper usage of Eq. (3) for the case of direct-detection frequency-scanned φ-OTDR is addressed in great detail under section 4.2.

The parameter β (mentioned in Eq. (3)) can be solved either numerically or analytically. Prior knowledge of the shape of the power density of the signal under consideration is not required when the numerical approach is followed. However, to obtain an analytical solution for β, an expression for the power density needs to be formulated. In a previous work presented in [36], the electrical power spectrum of the back-scattered light in direct-detection φ-OTDR (which can be calculated from the auto-convolution of the optical power density of the input pulse) for rectangular and sinc input pulses are given theoretically and validated experimentally. In the case of a rectangular input pulse, the analytical expression for the electrical sinc-shaped power density is given in [36]. However, this expression cannot be used in this study due to the fact that the signal under consideration for estimating the FS using cross-correlation is not the direct time-domain trace. In addition, the time-domain signals and the artificially-constructed signals are not related by ergodicity which means that the power densities will not yield the same distribution. Thus far, the power density of the artificially-constructed signal used in cross-correlation in direct-detection frequency-scanned φ-OTDR has not been investigated in any of the previous works. It is found that the power density for this artificially-constructed signal (with a rectangular input pulse to the fibre) has a triangular shape (illustrated in Fig. 2). The graph shows the summation of the power densities at each fibre position creating a smooth curve that manifests the actual shape of the power density. It should be noted that the use of the normalised frequency for the x-axis is for the generality of the concept, and will be further elaborated in section 4.2. The triangular-shaped power density is expected in this case because the artificially-constructed signal can be assimilated to a time-domain signal obtained using a sinc input pulse. Therefore, the power density of the artificially-constructed signal is logically given by the auto-correlation of a rectangular spectrum (for a sinc input pulse) which is triangular-shaped.

An analytical expression for β, given in Eq. (3), for a triangular-shaped power density is thus obtained similarly to [37], and takes the following form:

$$\beta = \frac{2\pi\,\tau}{\sqrt{6}} \tag{5}$$

Optics EXPRESS

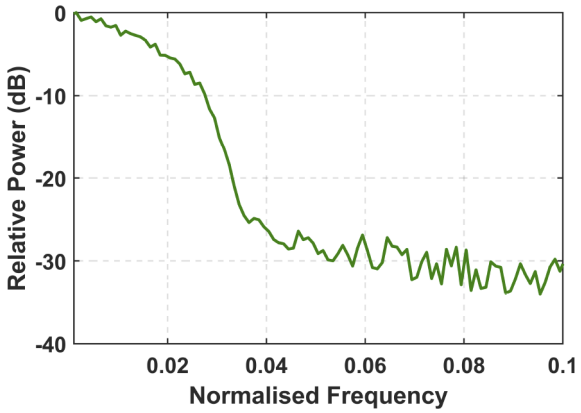

Fig. 2. Triangular-shaped power density of the signal under consideration as a function of the normalised frequency.

where τ is the pulse width (full width at half maximum) of the rectangular input pulse, which is also equivalent to the bandwidth of the power density of the artificially-constructed signal under consideration. Thus, the analytical solution for the FS uncertainty of a direct-detection frequency-scanned φ-OTDR system with a rectangular input pulse is given by:

$$\sigma = \frac{\sqrt{6}}{2\pi\tau M_o} \tag{6}$$

The above equation relates, in the case of a rectangular input probe pulse, the uncertainty in the FS estimation to the pulse width and the SNR of the signal.

3. Direct-detection frequency-scanned φ-OTDR setup

In this work an experimental setup for a direct-detection frequency-scanned φ-OTDR is employed to verify the expression for the measurement uncertainty in Eq. (6). The functionalities of all system components along with the devices used in the experimental setup will be thoroughly elaborated in this section.

In the experimental setup displayed on Fig. 3, a 1 MHz bandwidth distributed feedback (DFB) continuous-wave (CW) laser is used as the coherent light source of the φ-OTDR interrogation system utilised in this work. The stability of the laser is highly essential to avoid significant laser frequency drifts that could lead to additional uncertainty in the FS estimation. This, however, can be mitigated by technical improvement, such as laser stabilisation by locking, or by performing a fast measurement to make laser drifting negligible and measuring precisely the laser frequency when data is acquired. External intensity modulation of the CW light is achieved by means of a high extinction ratio (ER) semiconductor optical amplifier (SOA) leading to the generation of optical pulses, with desired spatial resolution for the measurement. The power of the pulse is then amplified by an Erbium-doped fibre amplifier (EDFA) followed by a variable attenuator, which serves to limit the power directed into the fibres to avoid nonlinear optical effects such as modulation instability.

The light then enters port 1 of a circulator, and passes through port 2 to travel into the fibre under test, which in this case is a $\sim$ 100 m single-mode fibre. A second amplification stage is required to boost the back-scattered signal before passing through a 1 nm optical filter, which is necessary to filter out the ASE noise generated by the EDFAs. The signal is then captured by a 125 MHz photo-detector, and acquired by a data acquisition card (DAQ) at a sampling rate of 500 MS/s.

Optics EXPRESS

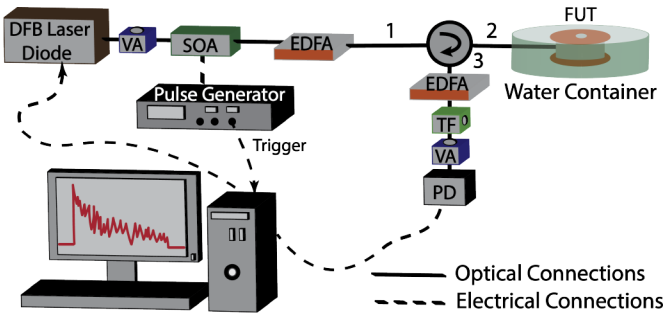

Fig. 3. Experimental setup of a frequency-scanned φ-OTDR using direct detection (DFB: Distributed feedback laser, SOA: Semiconductor optical amplifier, EDFA: Erbium-doped fibre amplifier, TF: Tunable filter, VA: Variable attenuator, PD: Photo-detector, FUT: Fibre Under Test).

The frequency sweep of the interrogating pulse is carried out by remotely controlling the laser driver, which in turn tunes the current of the DFB laser. The current scan is performed over 10 mA (3.2 GHz frequency range) with a step of 0.01 mA (3.2 MHz frequency step). Since there is no external perturbation applied to the fibre in the present scenario, the frequency scan range is limited to 3.2 GHz. It should be pointed out that the fibre is immersed in a large water bath to minimise any environmental influences occurring during the measurement.

4. Calculation of SNR and FS uncertainty

4.1. Calculation of the SNR in a φ-OTDR system

The SNR of a trace having an intensity distribution following an exponentially decaying probability density function (PDF) can be estimated by the following equation [29,38]:

$$M = \frac{\mu}{\sigma_n} \tag{7}$$

where M is the SNR, μ and σ_n are the mean and the standard deviation of the signal, respectively, for several consecutive measurements. Due to the jagged noise-like intensity pattern of the time-domain trace of a φ-OTDR system governed by an exponential PDF, Eq. (7) can be used for the rough estimation of the SNR since the limited sample leads to large uncertainties in the estimation of the mean μ. However, a more solid approach is proposed, for a more accurate estimation of the SNR of a φ-OTDR system. Using an incoherent OTDR setup, the back-reflection coefficient of the fibre is calculated by the following equation:

$$\alpha_{BS} = \frac{P_{BS_o}/P_{in_o}}{R_{sp}} \tag{8}$$

where α_{BS} is the back-reflection coefficient (in m^{-1}) measured at the input end of the fibre, P_{BS_o} is the back-scattered power obtained from the OTDR trace (as shown in Fig. 4), P_{in_o} is the input peak power to the fibre, and R_{sp} is the spatial resolution (in m) of the OTDR system (which is equivalent to half of the physical length of the interrogation pulse launched into the fibre). It should be noted that α_{BS} is the product of the absolute value of the Rayleigh back-scatter coefficient and the re-capture factor. In the case of a standard single-mode fibre, the α_{BS} is found to be −72.3 dB/m. The same method is utilised to calculate the α_{BS} of a different type of fibre under test as illustrated in Fig. 4. For the special fibre used in the current scenario, α_{BS} is calculated to be −64.3 dB/m. The difference in the value of α_{BS} is explained by the fact that

Optics EXPRESS

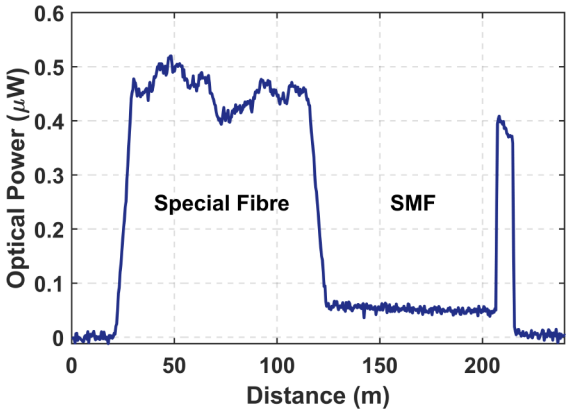

Fig. 4. Back-scattered OTDR trace in terms of back-scattered optical power (in μW) as a function of the fibre distance (in m) for two set of fibres with different SNR, namely special fibre and single-mode fibre (SMF). Note: The spike observed around 200 m is the reflection at the fibre end.

the core of this special fibre has been subjected to refractive index manipulation to enhance the back-scattering. Thus, α_{BS} serves as a metric parameter for a given fibre under test.

Once the back-reflection coefficient of the fibre under test is known, the back-scattered power (P_{BS_φ}) from the φ-OTDR system (depicted in Fig. 3), at a distance z in the fiber, can be simply calculated using the following standard equation [39]:

$$P_{BS_\varphi} = P_{in_\varphi}\, \alpha_{BS}\, R_{sp} \exp\left(-2\alpha z\right) \tag{9}$$

where α is the total attenuation coefficient of the fibre, and the factor 2 accounts for the round trip time that the light takes to reach the receiver at the input of the fibre. Using the conversion gain of the photo-detector utilised in the setup along with the gain and loss in optical power caused by the different optical components in the setup, the actual power reaching the photo-detector is determined. The value of the power obtained is the optical power (which is equivalent to the electrical voltage through the conversion gain of the photo-detector).

Different types of noises (such as optical and electrical noises) generated in the system will be additive noises to the signal, and can be quantified by computing the standard deviation, at each position in the fibre, of a number of time-domain traces. This value quantifies the overall noise electrical voltage in the system, which when multiplied with the conversion gain of the photo-detector results in an equivalent noise optical power value.

Thus, taking the ratio between the optical signal power and the noise power will yield the SNR (M_o) of the system. It should be mentioned that the SNR (M_e) is calculated as the integrated square of the electrical voltage. This means that the SNR calculated in this section (i.e., M_o) is equivalent to $\sqrt{M_e}$.

4.2. Calculation of the FS uncertainty numerically

As mentioned earlier, the traces used for performing the cross-correlation are signals which are artificially formed from the back-scattered optical intensity values for each fibre position as a function of all the pulse frequencies within the scanning range (lower part of Fig. 1(c)). However, it should be highlighted that throughout this study, no domain is defined for these artificially-constructed signals, and they are considered as signals with a specific number of samples. An example of such an artificially-constructed signal is shown in Fig. 5(a). In the present experiment, the total number of rows in the acquired 2-D array (representing the total

Optics EXPRESS

number of frequencies that are scanned in the frequency range) (upper part of Fig. 1(c)) is 1000. Therefore, the signal depicted in Fig. 5(a) has the same number of points as the number of frequencies in the scanning range which is 1000 samples. From the localised power density (Fig. 5(b)) of this constructed signal depicted in Fig. 5(a), the term β in Eq. (3) is calculated. The x-axis of Fig. 5(b) is expressed in the units of normalised frequency (cycles/sample) where the axis is basically normalised by the step size (Δf) of the artificially-constructed signal. Utilising the normalised frequency here is merely to present the concept in a rather simple and general manner that is independent of the step size. This is the most general approach which can be followed for the calculation of β. In this approach, no prerequisite information about the power density of the artificially-constructed signals is required. Finally, the value of the FS uncertainty (σ) obtained in Eq. (3) is then scaled back by the original frequency scan step Δf such that the absolute value and the proper unit of σ are yielded.

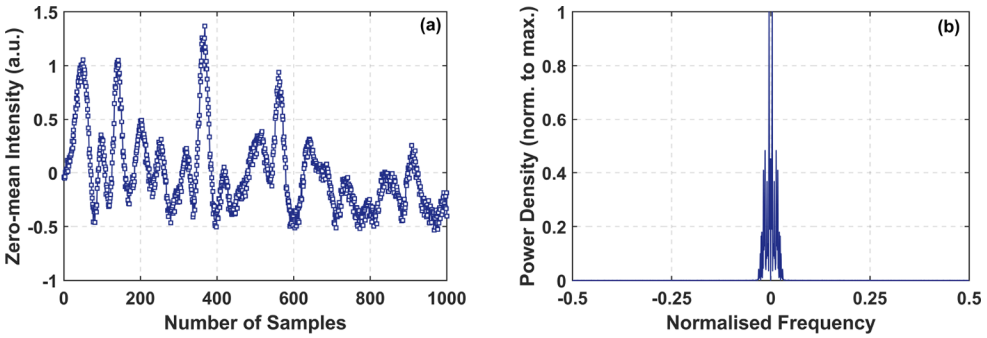

Fig. 5. (a) Back-scattered zero-mean intensity; (b) Localised power density (norm. to max.) of the signal in (a) as a function of the normalised frequency.

5. Experimental verification of the theoretical expressions

The absolute method of calculation of the SNR presented in section 4.1 for a φ-OTDR system is compared to the conventional method of SNR estimation for a trace following an exponential PDF. As illustrated in Fig. 6, the calculated SNR from the φ-OTDR time-domain traces using Eq. (6) and the theoretical model resulted in nearly the same values. This can be explained as follows: in the case of an OTDR, since an incoherent light source is used, the interrogating input pulse will have a short coherence length unlike the coherent light pulse in the case of the φ-OTDR. This makes the PDF of the OTDR time-domain trace follow a Gaussian distribution with significantly lower variance [40,41]. Thus, the time-domain trace of the OTDR appears to be like in Fig. 4, with the mean value of the time-domain trace obtained from the peak of the Gaussian distribution. For the case of the φ-OTDR, the interrogating input pulse is highly coherent, making the time-domain trace follow an exponentially decaying PDF. The expected value (mean) of the exponentially decaying PDF of the time-domain trace will give the average intensity of the back-scattered light. This implies that the mean value of the back-scattered intensity obtained from the time-domain traces of the OTDR and the φ-OTDR are equivalent. Thus, the SNR calculated using Eq. (6) or the proposed model will yield nearly the same result. The comparison assures that Eq. (6) can be followed for a rough estimation of the SNR even for a jagged intensity profile like in the case of a φ-OTDR system.

As explained in 2.2, an analytical expression is proposed to understand the influence of two main system parameters on the measurement accuracy of the φ-OTDR, while estimated using cross-correlation. The expression for calculating β given in Eq. (4) can be solved either analytically (as given in section 2.2) or numerically (as given in section 4.2). The former requires

Optics EXPRESS

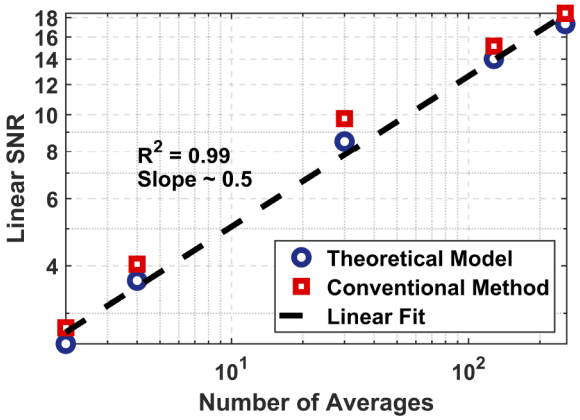

Fig. 6. Log-log plot of SNR versus number of averages; blue dashed line: calculated SNR using the theoretical model presented in section 4., red squares: calculated SNR using the mean value of the jagged time-domain trace divided by the standard deviation of 20 time-domain traces.

a prior knowledge about the shape of the power density of the artificially-constructed trace, unlike in the case of the latter. When the expression for β is solved numerically, the values obtained for β are normalised by the step size of the artificially-constructed signal, hence an associated normalised parameter $\bar{\beta} = \beta \times \Delta f$ is introduced, and will be used in some figures in the manuscript hereafter.

From the numerical calculations, it is found that the value of $\bar{\beta}$ is varying with respect to the SNR as depicted in Fig. 7. This phenomenon is quite ambiguous, but will be clearly elaborated later on in this section.

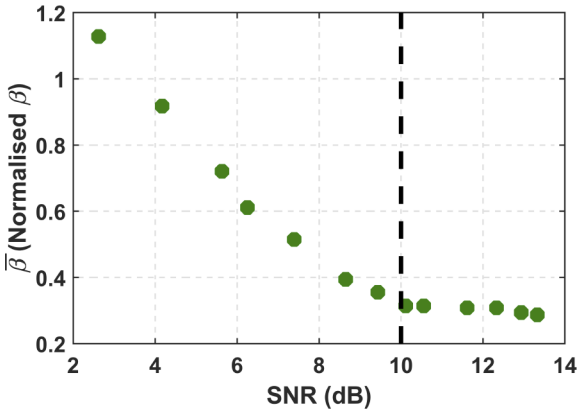

Fig. 7. Graph showing the dependency of $\bar{\beta}$ on the SNR. The black dashed line marks the SNR (~10 dB) at which the $\bar{\beta}$ starts being constant which means that it is not dependent on the SNR anymore.

To evaluate this dependency of $\bar{\beta}$ on the SNR, the SNR is varied keeping the pulse width a constant at 10 ns (corresponding to a spatial resolution of 1 m) during the experiment. Figure 8 illustrates the impact of the SNR on the power density. It is quite visible from the figure that a higher SNR yielded a higher amplitude of the power density. $\bar{\beta}$, however, is normalised, hence the change in the amplitude of the power density through the SNR variation is cancelled

Optics EXPRESS

out. Since $\bar{\beta}$ is derived under the assumption that SNR>>1, the presence of noise can bring unexpected ambiguities in the value of $\bar{\beta}$, implying that the square root of the second moment of the normalised power density will be higher for low SNR values. Figure 8(b) depicts $\bar{\beta}$ corresponding to low and high SNR conditions. When the SNR is low, the square root of the second moment of the power density, i.e., $\bar{\beta}$ is high. Alternatively, when the SNR is higher, $\bar{\beta}$ is low and it will remain a constant for even higher SNR values (as shown in Fig. 7). This results in an SNR-dependent $\bar{\beta}$ in the low SNR regime, whereas as per the proposed model it should be independent of the SNR. The latter condition is valid only when the SNR is relatively high, and in the present case this value is found to be around 10 dB (illustrated in Fig. 7). The constant value of the $\bar{\beta}$ is found accordingly to be around ~0.25.

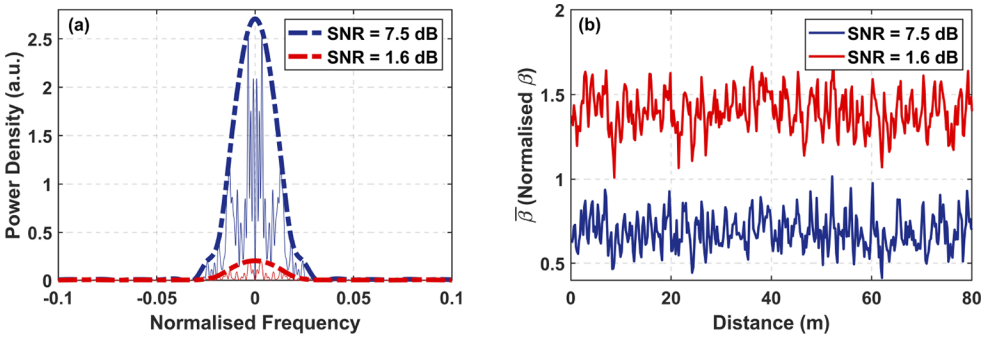

Fig. 8. Graphs showing: (a) the localised power density as a function of frequency for two different signal strengths (solid lines), the envelopes of the power densities (dashed lines); and (b) the square root of the second moment of the power densities ($\bar{\beta}$) in (a) as a function of distance.

It ought to be remarked that a significant discrepancy between the FS uncertainty/measurement accuracy calculated from the model and that from the experiment will occur (in the low SNR regime) if the σ is calculated with noise-dependent $\bar{\beta}$. However, fixing the $\bar{\beta}$ to a constant value of ~0.25 in all SNR conditions will result in perfectly-matching experimental and theoretical values, which indicates that the model is valid for all SNR cases as can be seen in Fig. 9. The value of $\bar{\beta}$ calculated numerically has to be de-normalised as follows $\beta = \bar{\beta} \times \frac{1}{\Delta f}$. Since $\Delta f = 3.2$ MHz in our case the value of $\beta \sim 78$ ns yielded can be then taken as a constant for any φ-OTDR system using 10 ns rectangular pulses. Other pulse widths can be calculated using a simple proportion.

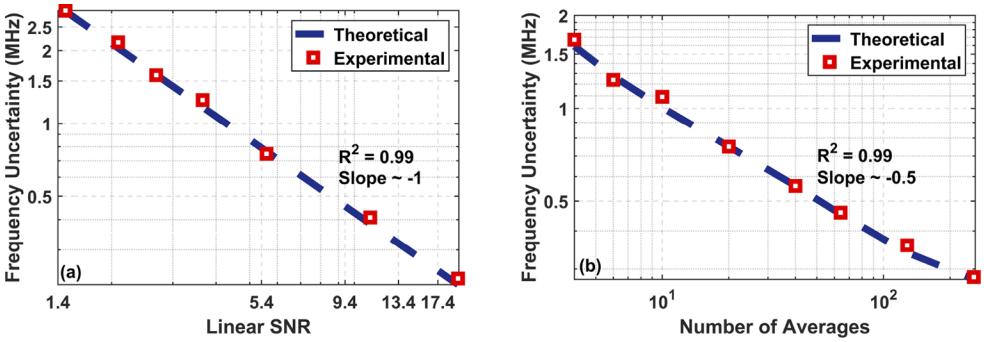

Fig. 9. Graphs represent the log-log plot of the frequency uncertainty as a function of (a) the optical power SNR (M_o); and (b) the number of averages.

Optics EXPRESS

To validate the expression for the FS uncertainty proposed in Eq. (3), various measurements are conducted along a ~100 m long standard single-mode fibre with 1 m spatial resolution. The SNR in the experiments is altered using two techniques; firstly by changing the input power to the fibre while keeping the averages a constant, and secondly by keeping a constant input power while increasing the number of averages. Figure 9(a) shows the FS uncertainty as a function of the SNR for the case in which the SNR is altered by varying the input power. As can be observed, the inverse proportionality between the FS uncertainty of the measurement and the SNR (M_o) proposed by the theoretical model is validated through the significantly well-matched theoretical and experimental values. In Fig. 9(b), the FS uncertainty is plotted against the number of averages showing the second case in which the SNR is varied by increasing the number of averages. As per the calculation from [17], the SNR is implicitly related to the number of averaged traces through the relationship: SNR $\propto \sqrt{N_{avg}}$ where N_{avg} is the number of time-averaged traces. Thus, applying this relationship to Eq. (3), the FS uncertainty is related to the number of averages by $1/\sqrt{N_{avg}}$ which is illustrated in Fig. 9(b). Figure 9(a) and (b) show a remarkable agreement between the measured FS uncertainty and the theoretically predicted FS uncertainty. This agreement thus confirms the inverse and inverse square root relationship of σ with the SNR and the number of averaged time-domain traces, respectively.

Another major parameter which plays a significant role in the FS estimation is the spatial resolution of the φ-OTDR system (pulse width of the interrogating input pulse). It is found from a number of experimental analyses that the uncertainty in the FS estimation using cross-correlation decreases with the increase of the pulse width. The experiment is performed by keeping all system parameters constant, and only varying the pulse width from 30 ns to 55 ns. From Eq. (8), it is obvious that an increase in the pulse width (thereby the spatial resolution) of the input pulse by a factor of 2 will increase the back-scattered power P_{BS_φ} by 3 dB, which will be reflected in the SNR as well. This implies that a change in the pulse width is coupled with a linear change in the SNR. In the theoretical model proposed here, the relationship between the FS uncertainty and the pulse width is reflected through the value β. Since these artificially-constructed signals can be thought of as a spectral response of the time-domain traces, and are not directly measured but artificially extracted from the time-domain traces, the alteration of the pulse width is reflected in the artificially-constructed signals as well. Thus, a narrower pulse width results in spectrally-broader individual features of the artificially-constructed signal (consecutive statistically-dependent points in the signal form one peak), as a result of the broader spectral distribution of the pulse. The power density of such an artificially-constructed signal is then calculated from the Fourier transform of the signal's auto-correlation function. Thus, it returns physically to the domain of the interrogating signal (time-domain). The full width at half maximum yielded for this power density is then linearly proportional to the pulse width used in the experiment. It should be highlighted and clearly understood that both, the interrogating signal and the power density of the artificially-constructed signal, are functions of the same domain and therefore vary jointly.

As given by the analytical expression in Eq. (4) for β for a rectangular input pulse, $\bar{\beta}$ of the power density linearly depends on the pulse width τ. Experimentally, this is demonstrated as an increment in the width of the normalised power density as illustrated in Fig. 10(a), implying that the square root of the second moment of the power density is proportional to the pulse width. Figure 10(b) shows the linear dependency of β and the pulse width of the interrogating pulse. It is, thus, confirmed that the larger the width of the interrogating pulse, the higher is the value of β. Finally, the influence of the pulse width on the FS uncertainty is analysed. The dependency of the FS uncertainty on the pulse width is expected to be inversely proportional as proposed in the model. However, since the SNR is also varied with respect to the pulse width, the dependence of the spatial resolution on the FS uncertainty is inverse square as validated through the experimental results given in Fig. 10(c).

Optics EXPRESS

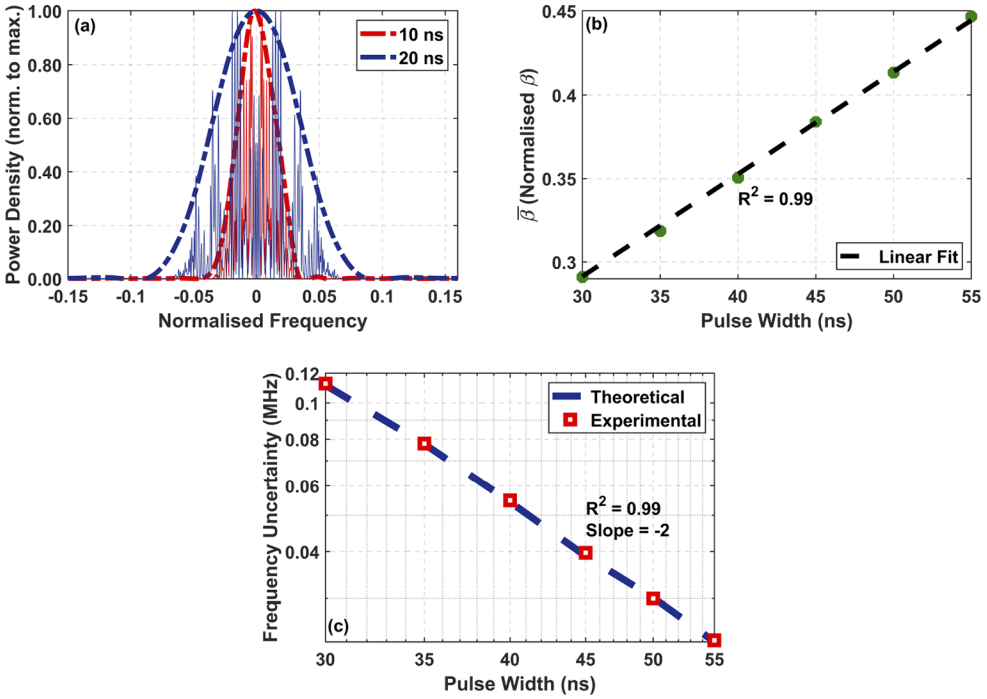

Fig. 10. Graph showing: (a) the localised power density as a function of frequency for different pulse widths (solid lines), the envelopes of the power densities (dashed lines); (b) $\bar{\beta}$ as a function of different pulse widths; and (c) the log-log plot of FS uncertainty as a function of different pulse widths.

To sum up, the influence of two key system parameters (SNR and spatial resolution) on the estimation of the FS using cross-correlation is evaluated properly through the presented analytical model and the experimental results. These experimental validations confirm that the proposed model for estimating the FS uncertainty for Rayleigh-based DOFS with the use of cross-correlation is based on a solid background, and can be used to predict the accuracy of such sensing systems. Besides, the model can be used as an efficient tool for optimising the experimental parameters to achieve the best system performance.

6. Conclusion

An analytical expression for the estimation of the frequency shift uncertainty in a direct-detection frequency-scanned φ-OTDR system is presented and validated for the first time, to the best of our knowledge, in this work. The expression, based on cross-correlation, evaluates the system performance through the investigation of the dependency of the frequency shift uncertainty/measurement accuracy on the following major measurement parameters: SNR and spatial resolution. According to the expression which is further validated through the experimental results, the measurement accuracy of the φ-OTDR system is inversely proportional to the SNR and the spatial resolution. In addition, the effective dependency of spatial resolution on the measurement accuracy is inverse square when the linear dependency of spatial resolution on the SNR is also taken into account. The proposed expression is valid in all cases of SNR and all different pulse widths, irrespective of the shape of the interrogating laser pulse and delivers a real quantitative prediction of the final uncertainty. Similar functional dependence of the uncertainty on SNR and pulse width is expected using other techniques to determine the FS,

Optics EXPRESS

such as the least-mean square method [15], though with possibly a different scaling factor to be determined in a further work. A rigorous calculation of the SNR of the jagged noise-like φ-OTDR trace is also proposed and compared to the conventional rough estimation of the SNR of a signal following an exponentially decaying distribution for the first time, to the best of our knowledge. The theoretically calculated SNR values match quite well with those obtained using the conventional method indicating that one can undoubtedly follow the conventional method for a rough estimation of the SNR.

Funding. Marie Sklodowska-Curie Actions (722509); Innosuisse - Schweizerische Agentur für Innovationsförderung (579292).

Disclosures. The authors declare that there is no conflict of interest.

Data availability. Data underlying the results presented in this paper are not publicly available at this time but may be obtained from the authors upon reasonable request.

References

1. A. Hartog, "Distributed fiber-optic sensors: principles and applications," in *Optical Fiber Sensor Technology*, (Springer, 2000), pp. 241–301.
2. A. Beisenova, A. Issatayeva, S. Sovetov, S. Korganbayev, M. Jelbuldina, Z. Ashikbayeva, W. Blanc, E. Schena, S. Sales, C. Molardi, and D. Tosi, "Multi-fiber distributed thermal profiling of minimally invasive thermal ablation with scattering-level multiplexing in mgo-doped fibers," Biomed. Opt. Express **10**(3), 1282–1296 (2019).
3. A. Hartog, *An Introduction to Distributed Optical Fibre Sensors* (CRC Press, 2017).
4. L. Thévenaz and M. Soto, "The making of a good Brillouin distributed fiber sensor," in *Fiber-Based Technologies and Applications*, (Optical Society of America, 2014), pp. FTh4D–1.
5. G. Milione, P. N. Ji, E. Ip, and T. Wang, "Method to increase the signal to noise ratio of distributed acoustic sensing by spatial averaging," U.S. patent 10,345,138 (9 July 2019).
6. W. Chen, J. Jiang, K. Liu, S. Wang, Z. Ma, Z. Ding, T. Xu, and T. Liu, "Coherent OTDR using flexible all-digital orthogonal phase code pulse for distributed sensing," IEEE Access **8**, 85395–85400 (2020).
7. Z. Wang, B. Zhang, J. Xiong, Y. Fu, S. Lin, J. Jiang, Y. Chen, Y. Wu, Q. Meng, and Y. Rao, "Distributed acoustic sensing based on pulse-coding phase-sensitive OTDR," IEEE Internet Things J. **6**(4), 6117–6124 (2019).
8. Z. Wang, J. Zeng, J. Li, M. Fan, H. Wu, F. Peng, L. Zhang, Y. Zhou, and Y. Rao, "Ultra-long phase-sensitive OTDR with hybrid distributed amplification," Opt. Lett. **39**(20), 5866–5869 (2014).
9. H. F. Martins, S. Martin-Lopez, P. Corredera, J. D. Ania-Casta non, O. Fraz ao, and M. Gonzalez-Herraez, "Distributed vibration sensing over 125 km with enhanced SNR using phi-OTDR over a URFL cavity," J. Lightwave Technol. **33**(12), 2628–2632 (2015).
10. T. Zhu, X. Xiao, Q. He, and D. Diao, "Enhancement of SNR and spatial resolution in φ-OTDR system by using two-dimensional edge detection method," J. Lightwave Technol. **31**(17), 2851–2856 (2013).
11. H. He, L. Shao, H. Li, W. Pan, B. Luo, X. Zou, and L. Yan, "SNR enhancement in phase-sensitive OTDR with adaptive 2-d bilateral filtering algorithm," IEEE Photonics J. **9**(6), 1–10 (2017).
12. S. Loranger, M. Gagné, V. Lambin-Iezzi, and R. Kashyap, "Rayleigh scatter based order of magnitude increase in distributed temperature and strain sensing by simple uv exposure of optical fibre," Sci. Rep. **5**(1), 11177 (2015).
13. Y. Xu, P. Lu, S. Gao, D. Xiang, S. Mihailov, and X. Bao, "Optical fiber random grating-based multiparameter sensor," Opt. Lett. **40**(23), 5514–5517 (2015).
14. P. S. Westbrook, T. Kremp, K. S. Feder, W. Ko, E. M. Monberg, H. Wu, D. A. Simoff, T. F. Taunay, and R. M. Ortiz, "Continuous multicore optical fiber grating arrays for distributed sensing applications," J. Lightwave Technol. **35**(6), 1248–1252 (2017).
15. L. Zhang, L. D. Costa, Z. Yang, M. A. Soto, M. Gonzalez-Herráez, and L. Thévenaz, "Analysis and reduction of large errors in Rayleigh-based distributed sensor," J. Lightwave Technol. **37**(18), 4710–4719 (2019).
16. J. Pastor-Graells, L. R. Cortés, M. R. Fernández-Ruiz, H. F. Martins, J. A. na, S. Martin-Lopez, and M. Gonzalez-Herraez, "SNR enhancement in high-resolution phase-sensitive OTDR systems using chirped pulse amplification concepts," Opt. Lett. **42**(9), 1728–1731 (2017).
17. M. A. Soto and L. Thévenaz, "Modeling and evaluating the performance of Brillouin distributed optical fiber sensors," Opt. Express **21**(25), 31347–31366 (2013).
18. L. Zhou, F. Wang, X. Wang, Y. Pan, Z. Sun, J. Hua, and X. Zhang, "Distributed strain and vibration sensing system based on phase-sensitive OTDR," IEEE Photonics Technol. Lett. **27**(17), 1884–1887 (2015).
19. D. Wang, J. Zou, Y. Wang, B. Jin, Q. Bai, X. Liu, and Y. Liu, "Distributed optical fiber low-frequency vibration detecting using cross-correlation spectrum analysis," J. Lightwave Technol. **38**(23), 6664–6670 (2020).
20. K. Markiewicz, J. Kaczorowski, Z. Yang, L. Szostkiewicz, A. Dominguez-Lopez, K. Wilczynski, M. Napierala, T. Nasilowski, and L. Thévenaz, "Frequency scanned phase sensitive optical time-domain reflectometry interrogation in multimode optical fibers," APL Photonics **5**(3), 031302 (2020).
21. C. Knapp and G. Carter, "The generalized correlation method for estimation of time delay," IEEE Trans. Acoust., Speech, Signal Process. **24**(4), 320–327 (1976).

Optics EXPRESS

22. M. Azaria and D. Hertz, "Time delay estimation by generalized cross correlation methods," IEEE Trans. Acoust., Speech, Signal Process. **32**(2), 280–285 (1984).
23. G. Carter, "Time delay estimation for passive sonar signal processing," IEEE Trans. Acoust., Speech, Signal Process. **29**(3), 463–470 (1981).
24. M. Froggatt and J. Moore, "High-spatial-resolution distributed strain measurement in optical fiber with Rayleigh scatter," Appl. Opt. **37**(10), 1735–1740 (1998).
25. Y. Koyamada, M. Imahama, K. Kubota, and K. Hogari, "Fiber-optic distributed strain and temperature sensing with very high measurand resolution over long range using coherent OTDR," J. Lightwave Technol. **27**(9), 1142–1146 (2009).
26. X. Lu, M. A. Soto, and L. Thévenaz, "Optimal detection bandwidth for phase-sensitive optical time-domain reflectometry," in *Sixth European Workshop on Optical Fibre Sensors*, vol. 9916 (International Society for Optics and Photonics, 2016), p. 99162N.
27. A. Alekseev, V. Vdovenko, B. Gorshkov, V. Potapov, and D. Simikin, "A phase-sensitive optical time-domain reflectometer with dual-pulse diverse frequency probe signal," Laser Phys. **25**(6), 065101 (2015).
28. P. Gysel and R. K. Staubli, "Spectral properties of Rayleigh backscattered light from single-mode fibers caused by a modulated probe signal," J. Lightwave Technol. **8**(12), 1792–1798 (1990).
29. H. Gabai and A. Eyal, "On the sensitivity of distributed acoustic sensing," Opt. Lett. **41**(24), 5648–5651 (2016).
30. P. M. Woodward, *Probability and information theory, with applications to radar* (Pergamon Press, 1953).
31. A. Quazi, "An overview on the time delay estimate in active and passive systems for target localization," IEEE Trans. Acoust., Speech, Signal Process. **29**(3), 527–533 (1981).
32. C. W. Helstrom, *Statistical theory of signal detection: international series of monographs in electronics and instrumentation*, vol. 9 (Elsevier, 2013).
33. P. M. Woodward, *Probability and information theory: with applications to radar* (Pergamon, 1953).
34. I. Cespedes, J. Ophir, and S. K. Alam, "The combined effect of signal decorrelation and random noise on the variance of time delay estimation," IEEE Trans. Ultrason., Ferroelect., Freq. Contr. **44**(1), 220–225 (1997).
35. P. Woodward, "Theory of radar information," Trans. IRE Prof. Group Inf. Theory **1**(1), 108–113 (1953).
36. X. Lu, M. A. Soto, L. Zhang, and L. Thévenaz, "Spectral properties of the signal in phase-sensitive optical time-domain reflectometry with direct detection," J. Lightwave Technol. **38**(6), 1513–1521 (2020).
37. L. Costa, H. F. Martins, S. Martín-López, M. R. Fernández-Ruiz, and M. González-Herráez, "Fully distributed optical fiber strain sensor with 10−12 $\varepsilon/\sqrt{\text{Hz}}$ sensitivity," J. Lightwave Technol. **37**(18), 4487–4495 (2019).
38. J. W. Goodman, *Statistical optics* (John Wiley & Sons, 2015).
39. L. Thevenaz, *Advanced fiber optics: concepts and technology* (EPFL press, 2011).
40. P. Healey, "Statistics of Rayleigh backscatter from a single-mode fiber," IEEE Trans. Commun. **35**(2), 210–214 (1987).
41. A. Masoudi and T. P. Newson, "Analysis of distributed optical fibre acoustic sensors through numerical modelling," Opt. Express **25**(25), 32021–32040 (2017).